Journal of Materials Chemistry A

Accepted Manuscript

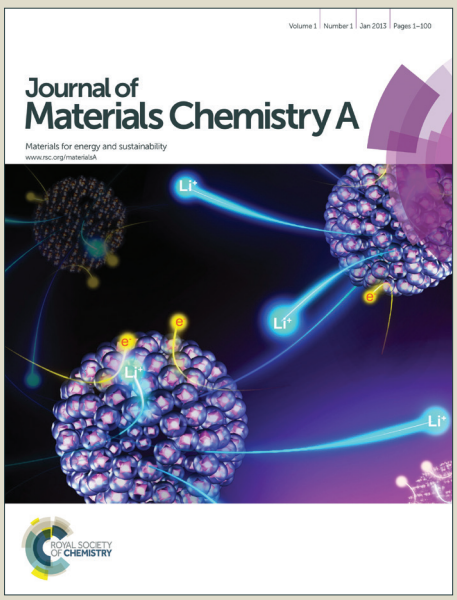

ROYAL SOCIETY OF CHEMISTRY

www.rsc.org/materialsA

Cite this: DOI: 10.1039/c0xx00000x

www.rsc.org/xxxxxx

ARTICLE TYPE

Synthesis of hexagonal MoO_3 nanorods and their electrochemical performance as anode materials for lithium-ion battery

Jianbin Zhou,[a] Ning Lin,[a] Liangbiao Wang,[a] Kailong Zhang, [a] Yongchun Zhu*[a] and Yitai Qian*[a]

Received (in XXX, XXX) Xth XXXXXXXXX 20XX, Accepted Xth XXXXXXXXX 20XX

DOI: 10.1039/b000000x

Hexagonal MoO_3 nanorods with an average diameter of 40 nm have been synthesized in the immiscible mixture of water and methylbenzene. Both the critic acid, which can chelate molybdic acid in water solution, and the interface reaction occurred between two phases of solution are favorable for the formation of hexagonal MoO_3 nanorods. As an anode material for lithium-ion battery, the hexagonal MoO_3 nanorods exhibit a capacity over 780 mA h g^{-1} after 150 cycles at 150 mA g^{-1}, which is higher than that of hexagonal MoO_3 microrods with diameters of 2-3 μm.

1. Introduction

Molybdenum trioxide (MoO_3) is an important transition metal oxide due to its many distinctive properties that can be applied in various fields, such as gas sensors,[1] photochromic materials,[2] catalysis[3] and recording materials.[4] Furthermore, MoO_3 materials are considered as the promising anode candidates for lithium-ion batteries (LIBs) with a high charge storage capability, which is about 1117 mA h g^{-1} and three times that of traditional graphite.[5-8]

Commonly, MoO_3 has three different crystalline polymorphs, including orthorhombic MoO_3 (α-MoO_3), monoclinic MoO_3 (β-MoO_3), and hexagonal MoO_3 (h-MoO_3). α-MoO_3 is a thermodynamically stable phase with a layered structure,[9,10] as shown in Scheme 1 (a) and (b). Because of this stable structure, α-MoO_3 has been widely studied as anode materials for LIBs. α-MoO_3 nanoparticles with diameters of 5-20 nm exhibited a durable Li^+ storage capacity of 630 mA h g^{-1} over 150 cycles at a rate of C/2.[11] After 100 cycles at 200 mA g^{-1}, the carbon nanotube-wired α-MoO_3 nanobelts retained a capacity of 421 mA h g^{-1}.[12] Ant-Cave-Structured MoO_3−Carbon microballs showed a capacity of 733 mA h g^{-1} after 300 cycles at 2000 mA g^{-1}.[13]

h-MoO_3, as a metastable crystalline polymorph, is formed by the zigzag chains of [MoO_6] octahedral, which is inter-linked through the *cis*-position,[14] as showed in Scheme 1(c) and (d). With regard to the chemical and crystal structure, h-MoO_3 possesses the same potential to be applied in LIBs. For example, h-MoO_3 microrods based graphene composite showed a capacity of 739 mA h g^{-1} after 30 cycles at 100 mA g^{-1}.[15] However, the poor kinetics of Li^+ diffusion and conductivity in bulk MoO_3 have severely restrained its electrochemical performances. As known, using nanostructured MoO_3 is a feasible method to resolve these issues. To date, various of h-MoO_3 nanostructures have been reported, including nanobelts,[16] nanorods,[17] nanoparticles,[18] nanoplates,[19] and so on. However, the study on the electrochemical performance of h-MoO_3 nano-materials as anode for LIBs was seldom reported.

Meantime, as to the synthesis of h-MoO_3 nano-materials, much attention has been paid to the hydrothermal method.[20-22] For example, h-MoO_3 nanoparticles with several tens of nanometers were prepared from sodium molybdate using hydrothermal synthesis and ultrasonication.[21] h-MoO_3 nanorods with diameter of ~500 nm were hydrothermal synthesized from ammonium paramolybdate.[22]

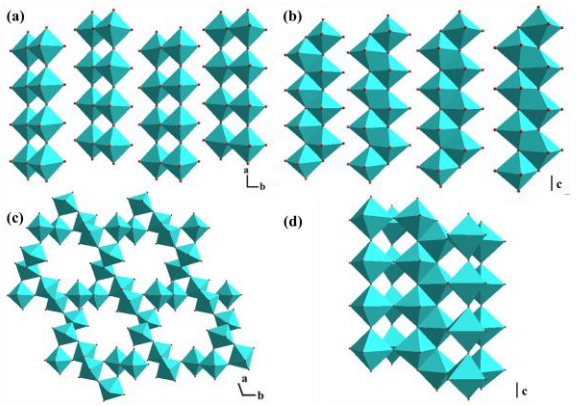

Scheme1. Schematic representation of α-MoO_3 ((a) and (b)), h-MoO_3 crystalline structure ((c) and (d)).

However, as previously reported, α-MoO_3 nanotubes can be synthesized through interface-mediated reaction.[23] Here, we have synthesized h-MoO_3 nanorods with an average diameter of 40 nm in the immiscible mixture of water and methylbenzene. In this reaction system, the added citric acid, complexing with molybdic acid in water, and the interface reaction may be favorable for the formation of h-MoO_3 nanorods. As anode materials for LIBs, the h-MoO_3 nanorods deliver a high reversible capacity of 780 mA h g^{-1} at 150 mA g^{-1} over 150 cycles and rate capability of 592.9, 500.4, 343.3 mA h g^{-1} at 300, 600 and 1000 mA g^{-1}, respectively. As a contrast, the h-MoO_3 microrods synthesized through other ways only retain 296.9 mA h g^{-1} at 150 mA g^{-1} after 30 cycles. The enhanced performance of h-MoO_3 nanorods could be attributed to the one-dimensional nanostructure of h-MoO_3.

2. Experimental

2.1 Preparation of h-MoO_3 nanorods

In a typical reaction process, 0.50 g of molybdic acid (H_2MoO_4) and 0.40 g of citric acid (H_4cit) dissolved in 20 mL deionized water were mixed with 10 mL methylbenzene, and then the as prepared mixture was stirred for 30 min at room temperature. After that, the mixed solution was transferred into autoclave and heated at 190 ^oC for 12 h. Then the autoclave was allowed to cool naturally, and the obtained product separated into two phases. The upper methylbenzene was deserted, and the lower turbid solution was centrifuged at 10000 rpm for 30 min. The collected bluish precipitate was redispersed in ethanol with sonication and centrifuged to remove methylbenzene residue. After dispersing of the precipitate in water, a centrifugation at 1000 rpm for 5 min was employed to remove the h-MoO_3 microrods and nanocrystals at the bottom of the centrifuge tube (ESI, Figure S1†). Further stepwise centrifugation with increasing speed and dispersing of the precipitate were conducted to remove H_4cit. Finally, the obtained product was dried in a vacuum oven at 60 ^oC overnight. The average yield of h-MoO_3 nanorods is 28.3 %, according to the results of five parallel experiments (ESI, Table S1).

2.2 Preparation of h-MoO_3 microrods

The h-MoO_3 microrods were synthesized through other method.[24] In a typical experiment, concentrated ammonium heptamolybdate tetrahydrate (0.88 g) was added into 10 mL deionized water under stirring. After that, concentrated H_2SO_4 (1.5 mol/L) was dropwise added into above solution, which was heated in a hot water bath at 100 ^oC and kept for 20 min. The collected precipitates were washed with deionized water several times and finally dried overnight at 30 ^oC.

2.3 Characterization

The phases of the samples were characterized by X-Ray diffraction (XRD, Philips X'Pert Super diffractometer with Cu Kα radiation (λ=1.54178Å)). The scanning electron microscopy (SEM) images were recorded on JEOL-JSM-6700F field emission scanning electron microscope with an accelerating voltage of 5 kV. The transmission electron microscopy (TEM) images were taken from Hitachi Model H-7650 transmission electron microscope with an accelerating voltage of 100 kV. The sample was analyzed by Fourier transformed infrared spectroscopy (FTIR) on Hyperion 3000 with the wavenumber ranging from 400 cm^{-1} to 2000 cm^{-1}. The chemical compositions and chemical states on surfaces of the sample were examined by X-Ray photoelectron spectroscopy (XPS) on GESCALAB KII - ray photoelectron spectrometer. Thermogravimetric analysis (TGA) and differential thermal analysis (DTA) were performed on SDT-Q600 under air condition at a heating rate of 10 ^oC/min from 25 ^oC to 600 ^oC.

2.4 Electrochemical measurements

Electrochemical properties were measured by using coin-type half cells (2016 R-type) in an argon filled glove box with lithium foil as the counter and reference electrode, celgard 2400 as the separator, and a solution of 1.0 M $LiPF_6$ in ethylene carbonate (EC)–diethyl carbonate (DEC) (1 : 1 by volume) as the electrolyte. For preparing working electrode, the active materials, acetylene black and poly (vinylidene diuoride) (PVDF) with a weight ratio of 80 : 10 : 10 were mixed homogeneously with N-methyl-2-pyrrolidone (NMP) and the slurry was pasted onto a copper foil and dried at 110 ^oC for 12 h in a vacuum oven. The mass of the active materials was controlled in the range of 2-3 mg. Galvanostatic charge–discharge was conducted by utilizing a battery tester (LANDCT2001A), which was cycled between 0.01 V and 3.0 V (vs. Li/Li^+) at 150 mA g^{-1}. A cyclic voltammogram (CV) was performed on electrochemical workstation (CHI660D) with a scanning rate of 0.1 mV s^{-1} with a voltage window of 0.01-3.0 V at room temperature. The electrochemical impedance spectroscopy (EIS) was performed on a CHI660D electrochemical workstation.

3. Results and discussion

The phase of the synthesized h-MoO_3 nanorods was characterized by XRD, as showed in Figure 1(a). All the diffraction peaks can be indexed to a hexagonal phase MoO_3 (lattice parameters a = 10.55 Å, c = 14.89 Å), which agrees well with the reported values (JCPDS 21-0569).[24,25] In Figure 1(a), the intensity ratio of $I_{(100)}/I_{(210)}$ is 3.6, which is larger than that of JCPDS 21-0569 with 2.0, indicating that the preferred orientation is {100} planes. The XRD pattern of h-MoO_3 microrods is presented in Figure S2 (a) †, which can also be indexed to JCPDS 21-0569.

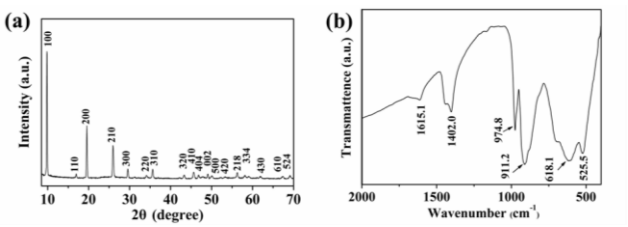

Figure 1. (a) XRD pattern and (b) FTIR spectrum of the h-MoO_3 nanorods.

Figure1 (b) shows the FTIR of the h-MoO_3 nanorods. The relatively sharp peaks at 974.8 and 911.2 cm^{-1} indicate the stretching of Mo=O double bond. The O−Mo−O stretching and bending with different Mo−O bond lengths at 618.1 and 525.5 cm^{-1}, respectively, match well with reference.[25] The peaks located at 1402.0 and 1615.1 cm^{-1} represent bending vibration of H−O−H and OH groups respectively, which imply the existence of crystalline water in the crystal of h-MoO_3 nanorods.[26]

XPS is conducted to evaluate the chemical compositions and chemical states of the surfaces of h-MoO_3 nanorods, as showed in Figure 2(a). The Mo 3d spectrum (Figure 2(b)) presents the 5/2-3/2 spin-orbit doublet for the Mo valence state, where the intense doublet at EB(Mo $3d_{5/2}$) = 233.15 eV and EB(Mo $3d_{3/2}$) = 236.3 eV corresponds to Mo^{6+}, in close agreement with the data found in literatures.[27,28] However, the appearance of low intensity doublet at EB (Mo $3d_{5/2}$)= 231.78 eV and EB (Mo $3d_{3/2}$)= 234.92 eV indicate the existence of a little part of Mo^{5+} on the surface of the sample.[27] According to ratio of peak-area, the fractional amounts of Mo^{6+} and Mo^{5+} are calculated to be 95 and 5 %,

respectively, indicating that the surface of the sample mostly consists of Mo^{6+}. It is reported that the existence of Mo^{5+} is caused by the deficiency of O^{2-} in the crystal structure of MoO_3, which can increase the electrical conductivity.[29]

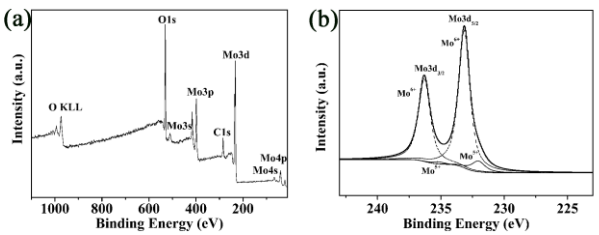

Figure 2. XPS spectra of as-obtained h-MoO_3 nanorods: (a) survey spectrum, (b) 3d core level regions of Mo^{6+} and Mo^{5+}.

To investigate the thermal behavior of h-MoO_3 nanorods, thermogravimetric analysis and differential thermal analysis (TGA/DTA) were conducted. According to Figure S3†, a broad exothermic peak on the differential thermal curve was observed from 430 to 500 °C corresponding to the phase change from h-MoO_3 to α-MoO_3, as the reported temperature of phase change is around 430 °C.[30] It's worth mentioning that an endothermic peak occurred on the differential thermal curve because of the loss of crystal water from h-MoO_3, which is in agreement with FTIR results. In addition, the uptrend on TG curve from 420 to 510 °C can be ascribed to the change of Mo_2O_5 to MoO_3.

Figure 3(a) shows the typical panoramic SEM image of h-MoO_3 nanorods, which exhibits a uniform morphology. In Figure 3(c), TEM image illustrates h-MoO_3 nanorods with a length range from microns to several hundred nanometers. The magnified SEM and TEM images, showed in Figure 3(b) and (d), distinctly disclose the feature of h-MoO_3 nanorods with an average diameter of 40 nm. Actually, we have tried to capture the HRTEM images of h-MoO_3 nanorods, but it is difficult due to the instability under the strong electron irradiation.[16,31] The SEM image of h-MoO_3 microrods is showed in Figure S3(b)†, which illustrates that the diameters are 2-3 μm.

To discover the growth mechanism of h-MoO_3 nanorods, two contrast experiments were conducted. The h-MoO_3 microrods were obtained in the absence of methylbenzene. Without adding citric acid (H_4cit), MoO_3 nanoparticles were harvested. The SEM images of the products obtained from contrast experiments are showed in Figure S4†. Based on above results, it is reasonable to conclude that the H_4cit and methylbenzene play decisive roles in the formation process of h-MoO_3 nanorods. Previous reports have shown that some unique structure of MoO_3, such as α-MoO_3 nanotube, can be formed through interface-mediated reactions, which have been well deployed for the synthesis and assembly of many other different kinds of nano-materials due to the confined growth environment provided by the interface.[32,33]

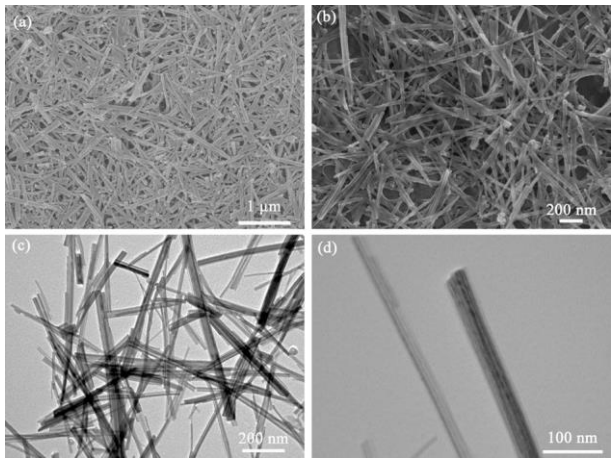

Figure 3. (a), (b) SEM images and (c), (d) TEM images of h-MoO_3 nanorods.

At the same time, on the basis of the knowledge that hydroxycarboxylic acids are strong molybdenum binders and many molybdenum based complex compounds with H_4cit have been reported,[34] therefore, we put forward a growth mechanism for the h-MoO_3 nanorods, as illustrated in scheme 2. At first, H_4cit would chelate molybdic acid (H_2MoO_4) in water solution and cause the formation of $(H_2MoO_4)_m(H_4cit)_n$.[35] When temperature reaches 190 °C, the H_2MoO_4 would be dehydrated. During this process, the coordination bond between H_2MoO_4 and H_4cit will become loose firstly, and then control the dehydration of H_2MoO_4 proceeding laxly. As reported, the amount of MoO_3 presented in water solution can be controlled by H_4cit,[36] which is beneficial for suppressing the crystals of MoO_3 from growing to large-sized crystals under appropriate condition. As methylbenzene and water are immiscible, the reaction can only take place at the interface between methylbenzene and water so that the growth dimension of MoO_3 is confined. Based on that, the MoO_3 crystal nucleuses, resulting from the dehydration of H_2MoO_4, will aggregate together to minimize surface energy and then self-assembled into arrays,[37] which grow toward the formation of h-MoO_3 nanorods.

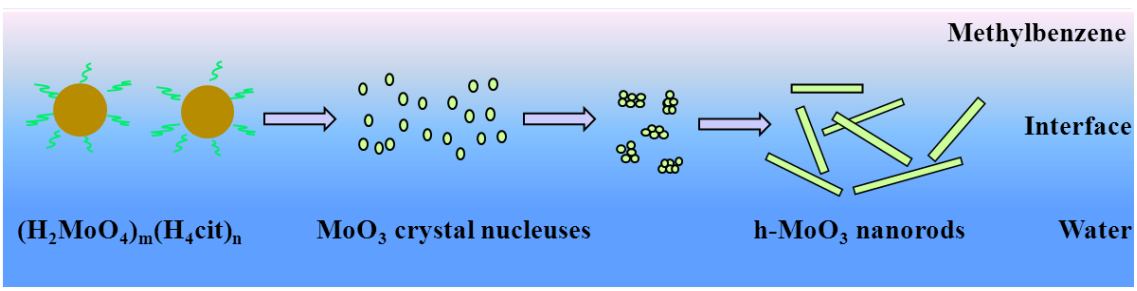

Schematic 2. The growth mechanism of h-MoO_3 nanorods

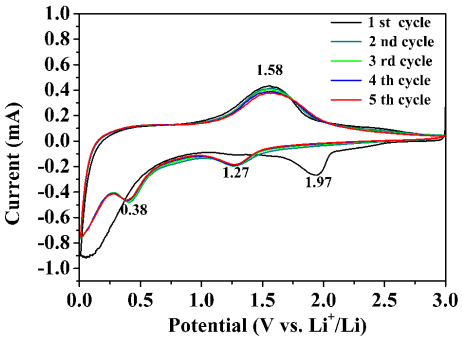

Figure 4. Cyclic voltammograms of h-MoO_3 nanorods at a scanning rate of 0.1 mV s^{-1} in the potential range of 0.01–3.0 V (vs. Li/Li^+).

The electrochemical properties of synthesized h-MoO_3 nano- and microrods were investigated as anodes for LIBs in Li half cells. Figure 4 shows the cyclic voltammetry (CV) curves of the h-MoO_3 nanorods from 1st−5th cycles at a scanning rate of 0.1 mV s^{-1} in the potential window of 0.01–3.0 V (vs. Li/Li^+), which exhibits the electrochemical information during the Li^+ insertion/extraction process. In the 1st cycle cathode part, a peak located at 1.97 V can be observed. The irreversible reduction peak at 1.97 V can be mainly ascribed to the irreversible intercalation of Li^+ into the crystal lattice and the structure change of MoO_3, which can't be fully recovered at the end of the first recharge.[38] Moreover, the irreversible reduction of the electrolyte and some other irreversible process can also lead to the formation of the irreversible reduction peaks that disappear in the following process. In the subsequent cycles, the reversible peaks located at 0.38 V, and 1.27 V can be ascribed to the process of lithiation in h-MoO_3 nanorods.[39] The major lithium extraction potential is around 1.58 V vs. Li/Li^+ . From 2nd cycle to 5th cycle, the CV curves are overlapped very well, which indicates the good reversible performance of h-MoO_3 nanorods anode.

Figure 5(a) exhibits the discharge-charge voltage–capacity curves of h-MoO_3 nanorods in the 1st, 50th, 100th and 150th cycles with a current density of 150 mA g^{-1} between a voltage limits of 0.01−3.0 V versus Li/Li^+. The first discharge potential plateau of h-MoO_3 nanorods around 2.0 V， as showed in Figure 5(a), is replaced by a group of sloping curves, mainly because of irreversible intercalation of Li^+ into the crystal lattice and the structure change during the first cycle. Owing to the same reasons mentioned above, the decay of capacity takes place from 1st cycle to 2nd cycle with an efficiency of 70.6 %. From 2nd to 150th cycles, no significant decline in capacity was detected, indicating the outstanding reversible electrochemical reaction between Li^+ and h-MoO_3 nanorods electrode. It is notable that the first lithiation capacity (1418.3 mA h g^{-1}), after fully discharged, has exceeded the theoretical capacity of MoO_3 (1117 mA h g^{-1}). However, the first charge capacity is 924.2 mA h g^{-1}, the large decay of capacity can be attributed to some part of the irreversible formation of Li_2O and some other irreversible processes as mentioned before.[40]

Furthermore, the cycling performance of the h-MoO_3 nano- and microrods, as presented in Figure 5(c), was evaluated by galvanostatic discharge-charge measurements with a voltage window from 0.01 V to 3.0 V at a current density of 150 mA h g^{-1}. As is shown, the cycling performance of h-MoO_3 nanorods is superior to that of microrods with a stabilized capacity of 779.9 mA h g^{-1} after 30 cycles. However, the capacity of h-MoO_3 microrods rapidly decreased to 296.9 mA h g^{-1}. In addition, h-MoO_3 nanorods show a high coulombic efficiency of about 99 % in Figure 5(c). During the discharging/charging process of h-MoO_3 nanorods, a slight decrease of the reversible capacity take

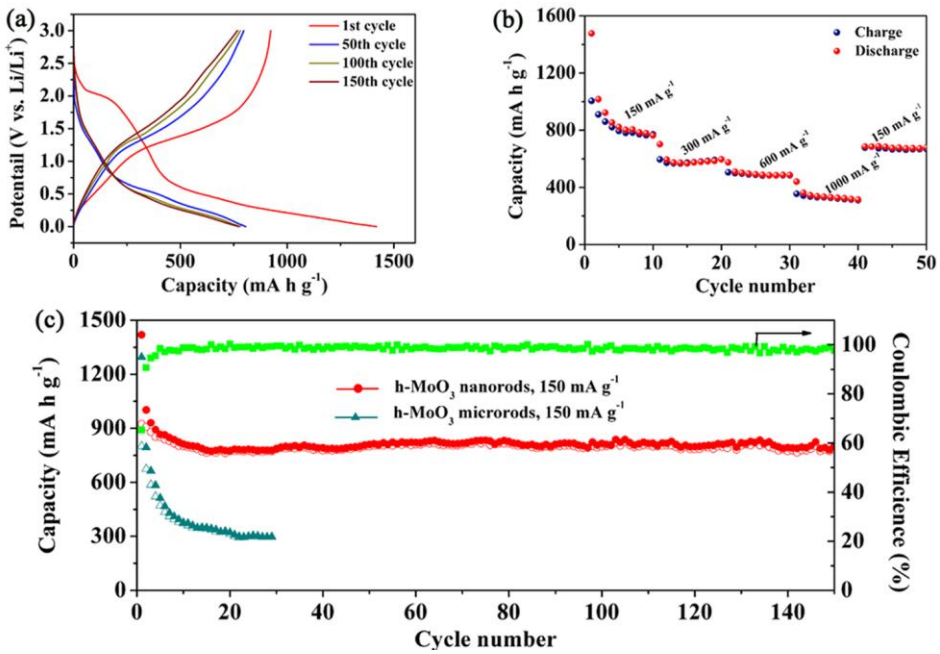

Figure 5. (a) Discharge-charge voltage–capacity curves of h-MoO_3 nanorods in the 1st, 2nd, 50th, 100th and 150th cycles at 150 mA g^{-1}. (b) Rate capability test at various current densities for h-MoO_3 nanorods. (c) Cycling performance of h-MoO_3 nano- and microrods at 150 mA g^{-1}.

place in the initial 5 cycles and then the reversible capacity stabilizes at 780 mA h g^{-1} after 150 cycles. Interestingly, an unconspicuous uptrend of the capacity can be found from 20th cycle to 134th cycle with an increased capacity from 761.9 mA h g^{-1} to 817.4 mA h g^{-1}, which can be commonly observed for transition metal oxides and normally attributed to the presence of a possible activation process during discharge and charge.[41,42] Besides the good cycling stability and high capacity, the rate performance, showed in Figure 5(b), is another important characteristic for high performance LIBs. At the current density of 300, 600, 1000 mA g^{-1}, the electrode of h-MoO_3 nanorods delivers the stable discharge capacity of 592.9, 500.4, 343.3 mA h g^{-1} respectively. After the high-rate discharge/charge cycling, an average capacity of 679.3 mA h g^{-1} can be restored when the current density is reduced to 150 mA g^{-1}, which exhibits the good rate performance of h-MoO_3 nanorods.

In order to further investigate the charge transport kinetics for the electrochemical properties of the h-MoO_3 nano- and microrods, electrochemical impedance were measured, as showed in Figure 6. It's well accepted that the diameter of the semicircle in high-to-medium frequency region is relevant for the charge transfer impedance in the electrode/electrolyte interface. Obviously, h-MoO_3 nanorods electrode shows much lower layer resistance than that of microrods electrode, which can be ascribed to the nanostructure of h-MoO_3 nanorods.

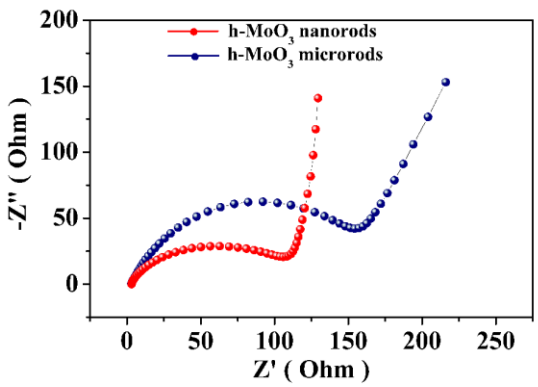

Figure 6. Electrochemical impedance spectra of electrodes made of h-MoO_3 nano- and microrods.

Compared with h-MoO_3 microrods, the h-MoO_3 nanorods with an average diameter of 40 nm exhibit enhanced reversible capacity and cycling stability. The better electrochemical performance can be mainly ascribed to the nanorod morphology of h-MoO_3. Firstly, with one-dimensional nanostructure, h-MoO_3 nanorods possess the advantage in releasing the strain of Li^+ insertion/extraction along the direction of one dimension,[43] which is beneficial for the maintenance of the morphology of h-MoO_3 nanorods and the cycling stability. For this part, we have also studied the morphology of h-MoO_3 nanorods (ESI, Figure S5 (a) †) and microrods (ESI, Figure S5 (b) †) after 150 cycles and 30 cycles by SEM, respectively. According to the SEM images, the morphology of h-MoO_3 nanorods was preserved, however, that of h-MoO_3 microrods was severely ruptured. As previously reported, α-MoO_3 nanobelts with width of 100-250 nm showed a much better electrochemical performance than bulk α-MoO_3 due to the nano-sized and well preserved morphology even at 5000 mA g^{-1} after 50 cycles.[44] What's more, the directional electron pathway along the one dimensional nano-materials exists in h-MoO_3 nanorods due to the quantum confinement effects.[45] These features are vital in improving the cycle stability and reversible capacity of the h-MoO_3 nanorods. In addition, because of the nano-sized diameter of h-MoO_3 nanorods, the shortened pathway of Li^+ is helpful for the enhanced charge transport kinetics and reduced electrochemical impedance.

4. Conclusion

In summary, we have synthesized h-MoO_3 nanorods with an average diameter of 40 nm in the immiscible mixture of water and methylbenzene. In this reaction system, the added citric acid, complexing with molybdic acid in water, and the interface reaction may be favorable for the formation of h-MoO_3 nanorods. As the anode material for LIBs, h-MoO_3 nanorods exhibit high capacity, cycling stability, good rate performance and low electrochemical impedance. The improved electrochemical performances can be ascribed to the one-dimensional nanorods morphology of h-MoO_3.

Acknowledgments

The authors would like to appreciate the financial support from the 973 Project of China (No. 2011CB935901), and the National Natural Science Fund of China (No. 91022033, 21201158).

Notes and references

[a] *Hefei National Laboratory for Physical Science at Microscale, University of Science and Technology of China, Hefei, 230026, P.R. China. Tel: +86-551-63601589; E-mail: ychzhu@ustc.edu.cn; ytqian@ustc.edu.cn.*

† Electronic Supplementary Information (ESI) available. See DOI: 10.1039/b000000x/

1 Z. W. Pan, Z. R. Dai, Z. L. Wang. *Science*, 2001, **291**, 1947.
2 J. N. Yao, K. Hashimoto, A. Fujishima. *Nature*, 1992, **355**, 624.
3 Y. S. Yoon, W. Ueda, Y. Morooka. *Catal. Lett.*, 1995, **35**, 57.
4 H. C. Zeng. *Inorg. Chem.*, 1998, **37**, 1967.
5 J. Chen, L. Xu, W. Li, X. Gou. *Adv. Mater.*, 2005, **17**, 582.
6 C. Ban, Z. Wu, D. T. Gillaspie, L. Chen, Y. Yan, J. L. Blackburn, A. C. Dillon. *Adv. Mater.*, 2010, **22**, 145.
7 A. M. Cao, J. S. Hu, H. P. Liang, L. J. Wan. *Angew. Chem. Int. Ed.*, 2005, **44**, 4391.
8 H. W. Shim, Y. H. Jin, S. D. Seo, S. H. Lee, D. W. Kim. *ACS Nano*, 2010, **5**, 443.
9 X. L. Li, J. F. Liu, Y. D. Li. *Appl. Phys. Lett.*, 2002, **81**, 4832.
10 K. Kalantarzadeh, J. S. Tang, M. S. Wang, K. L. Wang, A. Shailos, K. Galatsis, R. Kojima, V. Strong, A. Lech, W. Wlodarski, R. B. Kaner. *Nanoscale*, 2010, **2**, 429.
11 S. H. Lee, Y. H. Kim, R. Deshpande, P. A. Parilla, E. Whitney, D. T. Gillaspie, K. M. Jones, A. H. Mahan, S. B. Zhang, A. C. Dillon. *Adv. Mater.*, 2008, **20**, 3627.

12 J.F. Ni, G. B, Wang, J. Yang, D. L. Gao, J. T Chen, L. J. Gao, Y. Li. *J. Power Sources*, 2014, **247**, 90.
13 Y. N. Ko, S. B. Park, K. Y. Jung, Y. C. Kang. *Nano Lett.*, 2013, **13**, 5462.
14 I. P. Olenkova, L. M. Plyasova, S. D. Kirik. React. Kinet. *Catal. Lett.*, 1981, **16**, 81.
15 Q. W. Tang, L. Wang, K. L. Zhu, Z. Q. Shan, X. Qin. *Mater.Lett.*, 2013, 100, 127.
16 L. Zheng, Y. Xu, D. Jin, Y. Xie. *Chem. Mater.*, 2009, **21**, 5681.
17 Z. Z. Wu, D. Z. Wang, X. Liang, A. K. Sun. *Ultrason Sonochem.*, 2011, **18**, 288.
18 A. Chithambararaj, A. C. Bose. *J. Alloys. Compd*., 2011, **509**, 8105.
19 W. Tang, L. L. Liu, S. Tian, L. Li, Y. B. Yue, Y. P. Wu, K. Zhu. *Chem. Commun.*, 2011, **47**, 10058.
20 X. F. Yang, H. Y. Ding, D. Zhang, X. H. Yan, C. Y. Lu, J. L. Qin, R. X. Zhang, H. Tang, H. J. Song. *Cryst. Res. Technol.*, 2011, **46**, 1195.
21 Y. D. Xu, L. L. Xie, Y. J. Zhang, X. Y. Cao. *Electron. Mater. Lett.*, 2013, **9**, 693.
22 V. V. Atuchin, T. A. Gavrilova, V. G. Kostrovsky, L. D. Pokrovsky, I. B. Troitskaia, *Inorg. Mater.*, 2008, **44**, 622.
23 S. Hu, X, Wang. *J. Am. Chem. Soc.*, 2008, **130**, 8126.
24 W. Z. Pan, R. Y. Tian, H. Jin, Y. J. Guo, L. P. Zhang, X. C. Wu, L.N. Zhang, Z. H. Han, G. Y. Liu, J. B. Li, G. H. Rao, H. F. Wang, W. G. Chu. *Chem. Mater.*, 2010, **22**, 6202.
25 J. M. Song, X. M. Ni, L. S. Gao, H. G. Zheng. *Mater. Chem. Phys.*, 2007, **102**, 245.
26 J. D. Guo, P. Zavalij, M. S. Whittingham. *J. Solid State Chem.*, 1995, **117**, 323.
27 J. Zhou, J. Zhu, M. H. Yu, X. D. Huang, Z. Li, Y. H. Wang, C. Z. Yu. *J. Phys. Chem. C*, 2010, **114**, 20947.
28 J. Ś. Mrowiecka, S. Diesbach, V. Maurice, S. Zanna, L. Klein, E. Briand, I. Vickridge, P. Marcus. *J. Phys. Chem. C*, 2008, **112**, 11050.
29 F. Werfel, E. Minni. *J. Phys. C: Solid State Phys.*, 1983, **16**, 6091.
30 S. L. Bai，S. Chen, L. Y. Chen, K. W. Zhan, R. X. Luo, D. Q. Li, C. C. Liu. *Sens. Actuators, B-Chem.*, 2012, **174**, 51.
31 X. K. Hu, D. K. Ma, J. B. Liang, Q. Xie, Y. C. Zhu, Y. T. Qian. *J. Phys. Chem. C*, 2007, **111**, 5882.
32 S. Hu, X. Ling, T. Lan, X. Wang. *Chem. Eur. J.*, 2010, **16**, 1889.
33 X. Wang, Q. Peng, Y. Li. Acc. *Chem. Res.*, 2007, **40**, 293.
34 Z. H. Zhou, H. L. Wan K. R. Tsai. *Polyhedron*, 1997, **16**, 75.
35 J. J. Cruywagen, E. A. Rohwer, G. F. S. Wessels. *Polyhedron*, 1995, **14**, 3481.
36 H. N. Wilson. *Analyst*, 1954, 79, 535.
37 Penn, R. L.; Banfield, J. F. *Science*, 1998, **281**, 969.
38 Y. Iriyama, T. Abe, M. Inaba, Z. Ogumi. *Solid State Ionics*, 2000, **135**, 95.
39 C. L. Liu, Y. Wang, C. Zhang, X. S. Li, W. S. Dong. *Mater. Chem. Phys.*, 2014, **143**, 1111.
40 Z. Q. Yuan, L. L. Si, D. H. Wei, L. Hu, Y. C. Zhu, X. N. Li, Y. T. Qian. *J. Phys. Chem. C*, 2014, **118**, 5091.
41 L.L. Wang, J. W. Liang, Y. C Zhu, T. Mei, X. Zhang, Q. Yang, Y. T. Qian. *Nanoscale*, 2013, **5**, 3627.
42 G. Q. Zhang, L. Yu, H. B. Wu, H. E. Hoster, X. W. Lou. *Adv. Mater.*, 2012, **24**, 4609.
43 C. K. Chan, X. F. Zhang, Y. Cui. *Nano Lett.*, 2008, **8**, 307.
44 L. Zhou, L. C. Yang, P. Yuan, J. Zou, Y. P. Wu, C. Z. Yu. J. *Phys. Chem. C*, 2010, **114**, 21868.
45 J. Jiang, Y. Y. Li, J. P. Liu, X. T. Huang. *Nanoscale*, 2011, **3**, 45.